Identification of a novel nitroflavone-based scaffold for designing mutant-selective EGFR tyrosine kinase inhibitors targeting T790M and C797S resistance in advanced NSCLC

(Article begins on next page)

26 December 2024

Identification of a novel nitroflavone-based scaffold for designing mutant-selective EGFR tyrosine kinase inhibitors targeting T790M and C797S resistance in advanced NSCLC

Minnelli Cristina[1], Laudadio Emiliano[2], Sorci Leonardo[2], Sabbatini Giulia[1], Galeazzi Roberta[1], Amici Adolfo[3], Semrau S. Marta[4], Storici Paola[4], Rinaldi Samuele[1], Stipa Pierluigi[2], Marcaccio Massimo[5], Mobbili Giovanna[1]

[1] Department of Life and Environmental Sciences, Marche Polytechnic University, 60131 Ancona, Italy; c.minnelli@staff.univpm.it (C.M.); giulia.sabbatini@univpm.it (G.S.); g.mobbili@univpm.it (G.M.); r.galeazzi@univpm.it (R.G.); s.rinaldi@univpm.it (S.R.)
[2] Department of Science and Engineering of Matter, Environment and Urban Planning, Marche Polytechnic University, 60131 Ancona, Italy; e.laudadio@staff.univpm.it (E.L.); l.sorci@staff.univpm.it (L.S.); p.stipa@univpm.it (P.S.)
[3] Department of Clinical Sciences, Section of Biochemistry, Biology and Physics, U Marche Polytechnic University, 60131 Ancona, Italy; a.amici@univpm.it (A.A.)
[4] Protein Facility, Structural Biology Lab, Elettra Sincrotrone Trieste S.C.p.A., 34149 Basovizza, Trieste, Italy; marta.semrau@elettra.eu (M.S.S.); paola.storici@elettra.eu (S.P.)
[5] Department of Chemistry G. Ciamician, University of Bologna, Via Selmi 2, Bologna, 40126, Italy; massimo.marcaccio@unibo.it (M.M)
* Correspondence: g.mobbili@univpm.it (G.M.)

Abstract

The inhibition of the Epidermal Growth Factor (EGFR) represents one of the most promising strategies in non-small cell lung cancer (NSCLC) therapy. The recently identified C797S mutation causes resistance of EGFR$^{L858R/T790M}$ against osimertinib, the latest approved third generation EGFR inhibitor. The identification of small molecules capable of selectively inhibiting the T790M mutations also in the late-onset C797S mutation is a desirable strategy and novel chemical structures might provide new insight in the overcoming resistance mechanisms. Here we report the identification of a novel mutant-selective privileged molecular core; guided by a structure-based drug design, a flavone skeleton has been rationally modified, and a virtual library generated. Reversible EGFR inhibitors targeting both L858R/T790M and L858R/T790M/C797S mutations with a higher affinity with respect to the wild type one are discovered via a three-track virtual screening. Selected hits were synthesized and tested in an activity-based enzyme assay against wild-type EGFR, L858R/T790M, as well as L858R/T790M/C797S. The results showed that a nitroflavone-based compound inhibits the phosphorylation of EGFR mutants at low-micromolar concentration showing selectivity over the wild type ones. Structurally similar flavone analogues have been synthesized and the following inhibition assays underlied the importance of both the presence and position of the nitrophenoxy moiety.

1. Introduction

Activating mutations in the Epidermal Growth Factor Receptor (EGFR) are one of the major drivers of non-small cell lung cancer (NSCLC). However, although some studies have shown very high response rates of EGFR-mutant tumours to tyrosine kinase inhibitors (TKIs), resistance mechanisms could interfere with their efficacy. The most common EGFR mutations are the in-frame deletion of five amino acids in the exon 19 (EGFR^{Del19}) and the point mutation in the exon 21 (EGFR^{L858R}), which are associated with a high response to the first-generation inhibitors. However, TKIs-resistance

frequently occurs. 60% of treated patients develop the secondary mutation on the gatekeeper T790M residue [1] which seems to be more inclined to coexist with EGFR[L858R] than with EGFR[Del19] [2]. Osimertinib, which is the latest FDA-approved TKI, selectively overcomes T790M by a covalent bond formation with C797; however, the tertiary mutation (C797S) in EGFR caused new drug resistance by preventing the covalent bond with the side chain of C797 [3]. The ongoing research has actively pursued the discovery of novel TKIs to overcome the osimertinib-resistance. The coadministration of EAI045, an allosteric EGFR inhibitor, with cetuximab is effective in the EGFR[T790M/C797S] mutant model inhibition [3,4]. However, cetuximab is not EGFR mutant–specific also determines the inhibition of wild type EGFR form and leads to the failure of the clinical trials [4,5]. Drug discovery efforts have identified novel TKIs that selectively target C797S [6] or that covalently bind to the catalytic and conserved K745 residue [7,8]. However, an effective therapeutic approach to overcome the acquired resistance to the third-generation inhibitors could be the identification of the ATP-competitive inhibitors that selectively target EGFR[L858R/T790M], also in the late-onset C797S mutation.

Here we report the design of a novel privileged molecular core specific for EGFR[L858R/T790M] and EGFR[L858R/T790M/C797S] with selectivity over the wild type. For this purpose, a flavone skeleton has been selected as starting structure for our *in silico* drug design (**Figure 1**). The flat hetero aromatic system is rationally modified by introducing several chemical groups able to interact with the key regions of the ATP-binding pocket. It is known that an effective EGFR inhibition is obtained with a compound anchored to the kinase hinge region (Q791-G797) through a bidentate hydrogen bond (HB) [9,10] and extended to the phosphate binding (PB) region [11] undertaking interactions with the catalytic residue (K745) [7,8]. Moreover, several inhibitors exploit the highly conserved D855 residue in the DFG motif located at the beginning of the activation loop, which is important for protein catalysis [12]. Since R858 and M790 represent the key differences between the mutants (EGFR[L858R/T790M] and EGFR[L858R/T790M/C797S]) and the wild type EGFR, additional interactions with these amino acids could lead us to obtain a mutant-selective TKIs. In this context, we add appropriate chemical groups to take advantage of the increased hydrophobicity imposed by T790M mutation and the hydrophilicity of arginine as opposed to leucine (L858R). To this end, a homemade virtual library was generated, and a three-track virtual screening was applied to identify compounds with a higher affinity toward both mutated forms ($E_{binding}$ < -10 kcal/mol) with respect to the wild type one ($E_{binding}$ > -7 kcal/mol) (**Figure 1**). The selected hits were therefore synthetized and tested in an activity-based enzyme assay against EGFR-wt, -L858R/T790M, as well as -L858R/T790M/C797S. From the results obtained, a nitroflavone-based compound inhibits the phosphorylation of EGFR mutants at low-micromolar concentration showing a selectivity over the wild type greater than 150. Then, we measured the

biochemical potencies of structurally similar flavone analogues that underlie the importance of both the presence and position of the nitrophenoxy moiety.
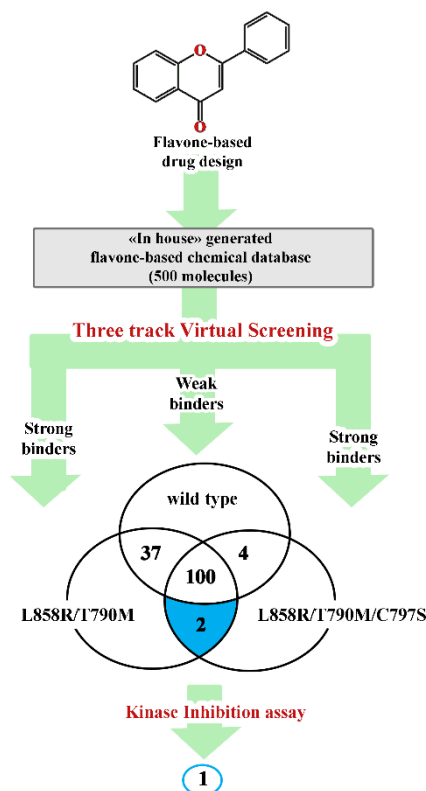

Figure 1. Flowchart for the discovery of mutant-selective EGFR inhibitors using the three-track virtual screening and enzyme inhibition assays.

2. Materials and methods

2.1 Materials

The materials and reagents employed in the synthetic procedures were purchased from Sigma Aldrich Co. (Stenheim, Germany) and used without purification. All solvents were analytically pure and dried before use. TLC were carried out on aluminum sheets precoated with silica gel 60 F254 (Merck). Column chromatography was performed using silica gel 60 (230–400 mesh).

High-resolution MS (HRMS) ESI analyses were performed on a Xevo G2-XSQTof (Waters) mass spectrometer. Mass spectrometric detection was performed in the in the positiveion mode. The ^{1}H and ^{13}C NMR spectra were recorded at 400 and 100 MHz, respectively, on a Agilent Technologies 400 MHz Premium Shielded spectrometer. Chemical shifts (δ) are reported in ppm relative to TMS and coupling constants (J) in Hz. Infrared spectra were made by diamond crystal ATR FTIR spectroscopy on a FT-IR Bruker Alpha and were expressed in wavenumber (cm−1). Insect cells and media for protein expression were from Expression Systems LLC (Davis - CA, USA), IMAC resin was from Qiagen, and protein chromatography columns from Cytiva.

2.2 Synthesis

2.2.1 2-hydroxy-5-(4-nitrophenoxy)acetophenone (2)

2,5-Dihydroxyacetophenone **1** (3.01 g, 19.8 mmol) was added to a solution of Cs_2CO_3 (12.90 g, 39.6 mmol, 2 eq) in 15 mL DMSO; after stirring for 30 min, 4-Fluoronitrobenzene (2.79 g, 19.8 mmol, 1 eq) was added and the reaction stirred at 50 °C for 24 h. The reaction mixture was then cooled, and water (150 mL) was added. pH was adjusted to 3 with 5 N HCl and the reaction extracted with EtOAc (3x300 mL). The combined organic layers were washed with brine, dried over Na_2SO_4, filtered and concentrated. The crude oil was purified by silica-gel chromatography with 20% EtOAc/cyclohexane to give the desired product **2** (3.8 g, Yield 70%) ^{1}H NMR (Acetone-D6, 400 MHz): δ 2.69 (s, 3H), 7.08 (d, J=9.0 Hz, 1 H), 7,14 (ddd, J=9.4 Hz, J=3.4 Hz, J=2.1 Hz, 2 H), 7.43 (dd, J=9.0 Hz, J=3.0 Hz, 1 H), 7.83 (d, J=3.0 Hz, 1 H), 8.25 (ddd, J=9.4 Hz, J=3.4 Hz, J=2.1 Hz, 2 H), 12.21 (s, OH). ^{13}C NMR (DMSO-d6, 100 MHz): δ 28.7, 117.1, 120.0, 122.0, 123.3, 126.6, 129.5, 142.5, 145.9, 158.4, 163.9, 203.5.

2.2.3. (E)-1-(2-hydroxy-5-(4-nitrophenoxy)phenyl)-3-(3-phenoxyphenyl)prop-2-en-1-one (3)

2-hydroxy-5-(4-nitrophenoxy)acetophenone **2** (1.20 g, 4.4 mmol) and 3-phenoxybenzaldehyde (0.87 g, 4.4 mmol) were added to a solution of potassium hydroxide (1.23 g, 22 mmol, 5 eq) in methanol (40 mL). The reaction was stirred for 48 h at 60 °C, and then cooled and acidified to pH 5–6 by adding 5% aqueous HCl. After extraction with EtOAc, the product was purified by column chromatography using silica gel as the stationary phase and 15% EtOAc/cyclohexane as mobile phase to give the desired compound **3** as a yellow solid. (1.7 g, Yield 86%). ^{1}H NMR (DMSO-d6, 500 MHz): 7.01(dd, J=0.8, J=8.6, 2H), 7.06 (dd, J=8.2, J=2.0, 1 H), 7.09-7.16 (m, 4H), 7.36-7,42 (m, 2H), 7.45 (dd, J=8.6, J=2.7, 2H), 7.65-7.73 (m, 2H), 7.84 (d, J=15.7, 1 H), 8.03 (d, J=15.7, 1 H), 8.18 (d, J=2.7, 1 H), 8.21-8.27 (m,2H), 12.40 (s, OH). ^{13}C NMR (DMSO-d6, 100 MHz): δ 116.9, 118.7, 119.8, 120.1, 121.7, 122.0, 123.2, 123.3, 123.9, 125.4, 126.6, 129.9, 130.4, 131.0, 137.0, 142.4, 145.0, 146.0, 157.1, 157.3, 159.8, 164.1, 193.2.

2.2.4. 6-(4-nitrophenoxy)-2-(3'-phenoxy)phenyl-4H-chromen-4-one (4)

Iodine (0.20 g, 0.8 mmol) was added to a solution of **3** (3.31 g, 7.3 mmol) in DMSO (20 mL) and the reaction mixture stirred at 130 °C for 6 h. After cooling to room temperature, the reaction was quenched with 0.5% $NaHSO_3$ (aq) (50 mL). The mixture was extracted with CH_2Cl_2 (3×50 mL) and the combined organic layers washed with brine (100 mL) and dried over Na_2SO_4. Volatiles were removed under reduced pressure to give a residue which was purified by silica gel column

chromatography (petroleum ether/ethyl acetate 1:1) to afford the desired compound **4** (2.6 g, Yield 78%) as a white solid. mp:161-162°C. ^{1}H NMR (DMSO-d6, 400 MHz): δ 7.06 (d, J=7.8, 2H), 7.07 (s, 1H), 7.13-7.24 (m, 4H), 7.40 (dd, J=8.6, J=7.8, 2H), 7.53-7.59 (m, 1H), 7.61(d, J=3.1, 1H), 7.67 (dd, J=9.0, J=3.1, 1H), 7.78-7.81 (m, 1H), 7.86-7.93 (m, 2H), 8.21-8.28 (m, 2H). ^{13}C NMR (DMSO-d6, 100 MHz): δ 106.9, 114.3, 116.7, 118.1, 118.7, 121.5, 121.6, 121.7, 123.9, 124.6, 126.2, 127.1, 130.2, 130.9, 133.0, 142.8, 151.8, 152.7, 156.3, 157.2, 162.0, 162.2, 176.5. IR(υmax/cm^{-1}): 1643 (C=O), 1347 (NO$_2$). Calcd. neutral mass for $C_{27}H_{17}NO_6$: 451.10559 Da. HRMS: m/z = 452.11 [M+H]$^+$, 474.10 [M+Na]$^+$.

2.2.5. 6-(4-aminophenoxy)-2-(3-phenoxyphenyl)-4H-chromen-4-one (5)

A solution of **4** (0.45 g, 1 mmol), Ni(acac)$_2$ (0.03 g, 0.1 mmol), and Poly(methylhydrosiloxane) (PMHS) (3 mL, 1.50 mmol) in dioxane (5 mL) was stirred at 80 °C under air atmosphere for the 12 h. After completion of the reaction, monitored by thin-layer chromatography (silica gel), the mixture was cooled to ambient temperature and purified by silica gel column chromatography using ethyl acetate/petroleum ether as eluent to obtain the desired compound **5** as light-yellow solid (140 mg, Yield 72%). mp:169-170°C. ^{1}H NMR (DMSO-d6, 500 MHz): δ 5.09 (broad s, 2H, NH$_2$), 6.64 (d, J=6.8, 2H), 6.84 (d, J=7.1, 2H), 7.02 (s, 1 H), 7.07-7.11 (m, 2H), 7.17-7.22 (m, 3H), 7.41-7.46 (m, 3H), 7.56-7.60 (m, 1H), 7.77-7.80 (m, 2H), 7,87-7,90 (m, 1H). ^{13}C NMR (DMSO-d6, 100 MHz): δ 107.1, 108.7, 115.5, 117.1, 119.2, 121.0, 121.8,122.0, 122.1, 124.3, 124.5, 124.6, 130.7, 131.4, 133.7, 145.4, 146.6, 151.3, 156.8, 157.2, 157.7, 162.1, 177.2. IR (υmax/cm^{-1}): 3441, 3344 (NH$_2$) 1626 (C=O). Calcd. neutral mass for $C_{21}H_{13}NO_5$: 359.07937 Da. HRMS: m/z = 422.14 [M+H]$^+$, 444.12 [M+Na]$^+$.

2.2.6. 6-(4-nitrophenoxy)-2-(phenyl)-4H-chromen-4-one (4a)

The product **4a** has been obtained starting from 2-hydroxy-5-(4-nitrophenoxy)acetophenone **2** (1.20 g, 4.4 mmol) and benzaldehyde (0.47 g, 4.4 mmol) following the same procedure as for compound **4**. (1.03 g, Yield 65%). mp:177-178°C. ^{1}H NMR (DMSO-d6, 400 MHz): δ 7.09 (s, 1 H), 7.21-7.28 (m, 2H), 7.56-7.67 (m, 4H), 7.71 (dd, J=9, J= 3.1, 1H), 7.95 (d, J=9, 1H), 8.11-8.16 (m, 2H), 8.25-8.31 (m, 2H). ^{13}C NMR (DMSO-d6, 100 MHz): δ 106.9, 114.8, 118.5, 121.9, 125.0, 126.7, 126.9, 127.5, 129.6, 131.4, 132.4, 143.2, 152.2, 153.2, 162.7, 163.3, 176.9 IR(υmax/cm^{-1}): 1639 (C=O), 1338 (NO$_2$). HRMS: m/z = 360.09[M+H]$^+$.

2.2.7 7-(4-nitrophenoxy)-2-(3'-phenoxy)phenyl-4H-chromen-4-one (4b)

The product **4b** has been obtained starting from 2,4-dihydroxyacetophenone (3.01 g, 19.8 mmol) following the same procedure as for compound **4.** (3.57 g, Yield 40%). mp:149-150°C ^{1}H NMR (DMSO-d6, 400 MHz): δ 7.03 (d, J=7.8, 2H), 7.05 (s, 1H), 7.11-7.18 (m, 2H), 7.26 (dd, J=2.4, J=9.0, 1H), 7.32-7.43 (m, 4H), 7.49-7.57 (m, 2H), 7.78-7.81 (m, 1H), 7.84-7.89 (m, 1H), 8.09 (d,J=9, 1H), 8.27-8.32 (m, 2H). ^{13}C NMR (DMSO-d6, 100 MHz): δ 107.9, 108.6, 117.3, 118.0, 119.0, 120.0, 120.6, 122.0, 122.1, 124.2, 126.7, 127.8, 130.6, 131.3, 133.4, 144.0, 156.8, 156.9, 157.5, 160.0, 161.2, 162.2, 176.8. IR($v$max/cm^{-1}): 1637 (C=O), 1349 (NO$_2$). Calcd. neutral mass for C$_{27}$H$_{17}$NO$_6$: 451.10559 Da. HRMS: m/z = 452.11 [M+H]$^+$, 474.10 [M+Na]$^+$.

2.2.8 5-(4-nitrophenoxy)-2-(3'-phenoxy)phenyl-4H-chromen-4-one (4c)

The product **4c** has been obtained starting from 2,6-dihydroxyacetophenone (3.01 g, 19.8 mmol) following the same procedure as for compound **4** (3.10 g, Yield 35%). mp:170-171°C. ^{1}H NMR (DMSO-d6, 500 MHz): δ 6.88 (s, 1H), 7.00-7.05 (m, 2 H), 7.06-7.10 (m, 2H), 7.16-7.21 (m, 2H), 7.25 (dd, J=0.9, J=7.9, 2H), 7.40-7.45 (m, 2H), 7.55-7.60 (m, 1H), 7.76-7.79 (m, 2H), 7.85-7.92 (m, 2H). ^{13}C NMR (DMSO-d6, 125 MHz): δ 109.1, 116.7, 117.1, 117.4, 117.6, 119.2, 119.8, 122.0, 122.2, 124.3, 126.3, 130.7, 131.4, 133.2, 135.4, 142.3, 151.7, 156.8, 157.7, 157.9, 161.0, 1643.2, 175.9. IR: 481.64, 693.38, 846.08, 997.36, 1213.49, 1256.39, 1346.66, 1466.05, 1515.57, 1588.71, 1608.83, 1638.57, 3042.43, 3092.16. IR($v$max/cm^{-1}): 1639 (C=O), 1347 (NO$_2$). Calcd. neutral mass for C$_{27}$H$_{17}$NO$_6$: 451.10559 Da. HRMS: m/z = 452.11 [M+H]$^+$, 474.10 [M+Na]$^+$.

2.3 EGFR modelling, ligand dataset preparation and three-track virtual screening

The TK domain of wild type EGFR, EGFRL858R, and EGFRL858R/T790M/C797S have been prepared using 3W2O pdb file [13]. A short loop lacking in the starting structure has been modelled, GalaxyWEB [14] has been used to model the junctions between carboxyl and amino terminal residues, while DISULFIND online server [15] has been used to predict the disulfide bonding state of cysteines and their disulfide connectivity. We generated the compounds starting from the flavone skeleton and adding the functional groups with UCSF Chimera [16]. All molecules have been parametrized using quantum mechanical calculations based on Density Functional Theory (DFT), using hybrid functional B3LYP and 6-311G** basis set; the ligands' Mulliken charges have been calculated and included in the ligand input file for subsequent docking calculations. The solvent effect was included by using the implicit water GB/SA solvation method [17]. Each designed TKI with the calculated charges and the most stable conformation has been added manually, to build up a homemade virtual library composed by more than 500 molecules. The binding mode of each molecule has been evaluated in the ATP-binding pocket of wild type EGFR, EGFR$^{L858R/T790M}$ and EGFR$^{L858R/T790M/C797S}$ with a semiflexible docking approach.

AutoDock Suite 4.2 [18] has been used to investigate the TKI-EGFR interactions. Autodocktools [19] has been used to add polar hydrogen atoms and partial charges for proteins, while TKIs charges have been obtained with previously described DFT method. Addsol tool has been used to assign atomic solvation parameters and fragmental volumes. Flexible torsions in the TKIs have been assigned with the Autotors module, and all dihedral angles were allowed to freely rotate. Affinity grid fields have been generated using the auxiliary program Autogrid, and the Mg^{2+} ions parameters have been included using the additional AD_4.1 bond package parameters.

Since the binding pocket in EGFR-TK domains has been already described [20–22], and the starting structures as well as the final designed TKIs were small molecules with few rotational degrees of freedom, a focused grid field of 60 x 54 x 68 $Å^3$ has been generated centered on EGFR-TK pockets with points spaced equally at 0.375 Å intervals. The docking calculations have been carried out by AMBER-based empirical free energy force field as implemented in Autodock 4.2 combined with a Lamarckian Genetic Algorithm (LGA), which provides a fast prediction of conformation and free energy. The number of GA runs is settled to 100, while the maximum number of top individuals that automatically survive is 0.1. The chosen step size for translation is 0.2 Å, and the energy evaluation is performed using a maximum number of evals of 25,000,000 (long). The resulting docked conformations have been clustered into groups with similar binding modes by a root mean square deviation (RMSD) clustering tolerance of 2 Å. The lowest energy conformations from the most populated clusters have been considered the most stable orientations. The sum of the intermolecular and the internal energies of the TKIs represents the docking energy, while the sum of the intermolecular and the torsional free energies is the free-binding energy [19]. This calculated free binding energy can be related to the inhibition constant (K_i) through the known thermodynamic equation $\Delta G = -RT \ln K_i$. PoseView program [23] has been used to plot the 2D TKIs binding poses. All the best binding modes of each compound have been selected on the basis of the highest population, which always corresponded to the lowest energy conformation, and by comparing the binding free energies obtained for the EGFR mutants with respect to the wild type one (lower than -10 kcal/mol and higher than -7.0 kcal/mol with respect the mutants and the wild type, respectively).

2.4. Molecular Dynamics Simulations

The complexes generated by three mutated EGFR forms with compound 4 that have been obtained by the previously described docking approach underwent 100 ns of molecular dynamics (MD) simulations following different steps of minimization and equilibration protocol with CHARMM36 force field [24]. The compound **4** has been modelled and parametrized using quantum mechanical calculations based on Density Functional Theory (DFT), using the hybrid functional B3LYP and 6-

311G** basis set to calculate the ligands' Mulliken charges and to compute a massive conformational analysis [17]. A simulation box of 120 Å^3 has been settled, including 54867 TIP3P water molecules to solve each system. Na^+ ions and Cl^- ions have been included explicitly to reach the physiological conditions (0.15 M NaCl) and to neutralize the net charge of the different EGFR proteins. Since the mutations can give different protein net charge, the number of ions added was different in relation to the total protonation state of the EGFR model. Solvation and ions were added using GROMACS 5.0.4 [25,26]. A minimization phase composed by 10,000 cycles of steepest descent followed by 5000 cycles of conjugate gradient minimization has been used to converge to the energy threshold of 1000 KJ/mol/nm. The following equilibration step has been adopted for each system with the aim to let the protein gradually accommodate in the salt-aqueous environment. In all runs, Verlet cutoff [27], combined with Particle Mesh Ewald (PME) for electrostatics [28] has been applied. The cutoff for the calculation of the Van der Waals force was set to 1.2 nm, while the force smoothly was switched to zero between 1.0 and 1.2 nm. Atom velocities have been generated at 310 K in the NVT ensemble using the Maxwell distribution function with generated random seed and a weak temperature coupling using the Berendsen thermostat. Time constant of 1 ps was applied to maintain the reference temperature (310 K) for the whole run. After equilibration simulation run of 2 ns, a switch to the NPT ensemble was carried out, maintaining the weak coupling also for pressure control (i.e., Berendsen barostat). For all simulation runs, the isotropic conditions have been settled with a reference pressure of 1 atm and a time constant for coupling of 5 ps. Position restraints have been applied to EGFR proteins, while a shift to the Nosé-Hoover [29] and Parrinello-Rahman algorithm for pressure coupling [30] has been operated for the production phase in NPT Ensemble. Then, a 100 ns-long MD simulation was run for each system implementing an accurate leapfrog algorithm or interacting Newton's equations of motion with a time step of 0.002 ps. The 2D binding modes of ATP at the end of MD simulations were detected using Discovery Studio, while the analysis of the simulations' trajectories was performed by means of the VMD [31] and CHIMERA software [16].

2.5. Enzyme inhibition assays

Recombinant EGFR proteins were purchased from SignalChem (T790M/C797S/L858R: E10-122VG) or produced (WT and L858R/T790M) as described [32]. Shortly, EGFR wild-type kinase domain was expressed in Sf9 insect cells and purified in 3 chromatographic steps: IMAC, anion exchange and size-exclusion (SEC). The final protein was frozen in 25 mM Hepes pH 8, 250 mM NaCl, 5% glycerol, 2 mM TCEP buffer and stored in aliquots at −80 °C until further use. The T790M/L858R mutations were inserted by the Q5 site-directed mutagenesis (New England Biolabs), and the protein was purified as the WT construct. The selected flavone derivatives were screened for

their ability to inhibit the tyrosine kinase activity of the EGFRs using the ADP-GloTM kinase assay. This discontinuous assay converts the ADP by-product formed upon EGFR activity to ATP which, in turn, is quantified with an ATP-dependent, luciferase/luciferin-based bioluminescent reaction. The kinase activity of each enzyme was measured in the presence of an ATP concentration of 10 µM, roughly equal to the K_m value. Compounds were tested in a 1% DMSO solution. For IC_{50} determination, the initial rate of the enzymatic reaction was measured at fixed ATP and peptide substrate in the absence and presence of various concentrations of inhibitors (typically 0-30 µM). Using GraphPad Prism, the IC_{50} value was determined by plotting the rates versus inhibitor concentration and fitting to the equation: $V_i = V_0/(1+[I]/IC_{50})$. V_0 and V_i represent initial rates in the absence and presence of inhibitors at concentration [I].

3. Results and discussion

3.1 Flavone-based drug design and virtual library generation

Among all the chemical skeletons used for the design of novel TKIs, flavone represents a compelling template (**Figure 1**): the flat hetero aromatic system, one of the common pharmacophoric features of EGFR-TKIs, can be easily used to place functional groups in the desired positions [33]. In this context, natural flavones such as apigenin and their derivatives seem to be very efficient in the inhibition of EGFR phosphorylation [34,35]. In order to introduce the appropriate chemical groups on the flavone skeleton, we firstly determined the flavone pose in the ATP binding pocket of the wild-type EGFR and EGFR[L858R/T790M] by a focused docking approach. The interactions involved have been investigated considering that many potent TKIs (e.g., quinazolines) exploit at least one hydrogen bond (HB) with the hinge region residues (M793 and/or Q791) [10,20,36]. Since our aim is to identify a scaffold that can target both L858R and T790M mutations independently of those acquiring the C797S, the design could be performed in the ATP binding pocket of EGFR[L858R/T790M].

From docking results, the most populated binding poses of the flavone molecule had 100%, 98%, and 100% of the conformational population in combination with wild-type, L858R/T790M, and L858R/T790M/C797S forms. These data indicate the presence of a univocal and reliable positioning for each studied EGFR receptor. On the other hand, important differences have been found in the flavone binding affinity in relation to the mutated EGFR type. In detail, an energy of -8.65 Kcal/mol has been calculated for the binding with wild-type form, and an increase to –5.67 Kcal/mol has been detected in association with the L858R/T790M form. This underlines a major affinity of the flavone for the wild-type. Finally, no remarked differences have been observed for the L858R/T790M/C797S form since the energy value was very similar to that calculated for the L858R/T790M form (-5.49

Kcal/mol). This means that the onset of the third mutation does not influence the binding mode of the flavone molecule inside the ATP-binding pocket of EGFR.

As shown in **Figure 2**, the flavone skeleton adopts a different orientation within the EGFR ATP-binding pockets. In the EGFR$^{L858R/T790M}$ (**Fig. 2B**), the flat hetero aromatic system is anchored to the M793, in the hinge region, through a HB with the carbonyl oxygen, and two π-alkyl interactions, respectively, with the B ring and the $C_2=C_3$ π system. The positioning of the ligand-receptor binding seems to be supported by the neighbouring hydrophobic interactions of the phenyl A ring with the hydrophobic region I (A743 and V730) and II (L844) of the ATP-binding site. Interestingly, the mutated gatekeeper residue M790 plays a key role in the stabilization of the flavone-EGFR complex by interacting with all the three rings of molecule (π-sulphur interaction with A and C rings and π-alkyl with B) (**Fig. 2A**). The importance of this interaction is underlined by the different binding mode observed in the wild-type EGFR form. In fact, the presence of the polar T790 induces the flavone to adopt a different orientation with respect to that observed in L858R/T790M form, moving it toward the phosphate binding region level (**Fig. 2B**). However, based on these results, the L858R does not seems to have a direct role on the flavone binding mode in these EGFR forms.
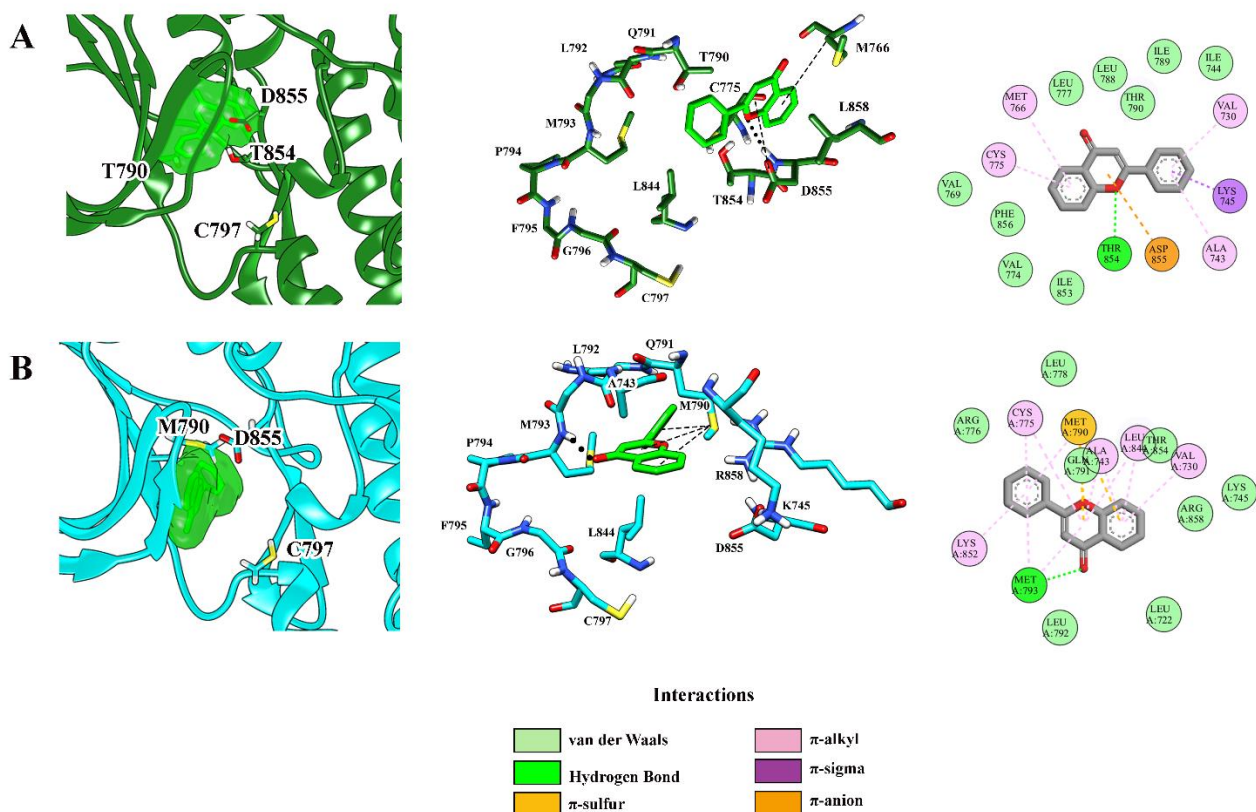

Figure 2. Focused docking of flavone in the ATP-binding site of (**A**) wild type EGFR (forest green) and (**B**) EGFR$^{L858R/T790M}$ (cyan). Carbon atoms of flavone are coloured in green. Hydrogen-bond and π-interactions are represented with black thick and thin dotted line lines, respectively. From left to right: surface representation of the flavone in the ATP-binding pocket, detailed binding mode of flavone in complex with EGFR receptors and 2D diagram drawn by Discovery Studio 4.5 representing the main residue involved in flavone-binding.

The next step is the rational modification of the flavone skeleton following the basic pharmacophoric features of EGFR-TK inhibitors [37] and exploring how the addition of several groups to the A and B rings can influence the bind of different flavone analogues in the binding pocket of the EGFR$^{L858R/T790M}$ (**Figure 3A**). It is noteworthy that the C2 and C3 of the B ring direct toward the vacant binding region comprising R858, K745, and D855 (**Figure 3B).** This peripheral binding pocket acts as PB region and represents a vulnerable target for some EGFR mutants because it includes the R858, a common mutated residue in the EGFR$^{L858R/T790M}$ and EGFR$^{L858R/T790M/C797S}$. In addition, the D855, belonging to the Asp-Phe-Gly (DFG) motif of the activation segment, represents, together with the catalytic K745 residue, a strategic target that can lead to a deregulation of kinase activity [38]. Therefore, a significant inhibitor potency could be obtained by the addition of a proper chemical moiety able to induce a strong interaction at this level. Due to the presence of positively charged amino acids containing H-donor atoms (K745 and R858), we hypothesize that more selective TKIs could be obtained by the introduction on the B ring of a phenyl head binding the selected residues by π-cation interactions and of an O-spacer able to promote the formation of HBs with the H-donor amino acids (**Figure 3C-D**). In addition, the presence of such an oxygen atom acting as an electron donator group could also strengthen the π-cation bond with lysine or arginine residues [39], stabilizing the positioning of the whole inhibitor skeleton at this peripheral binding pocket.

Regarding the A ring, C5, C6, and C7 point toward the hydrophobic region II (L844) near the hinge region. Therefore, the addition of a hydrophobic head could improve the stabilization of the inhibitor in the ATP-binding pocket. Moreover, a polar group linked to the hydrophobic moiety could act as H-acceptor or H-donor, strengthening the association with the hinge region. Following this rationale, a structure-based library of potential EGFR TKI has been generated for virtual screening.
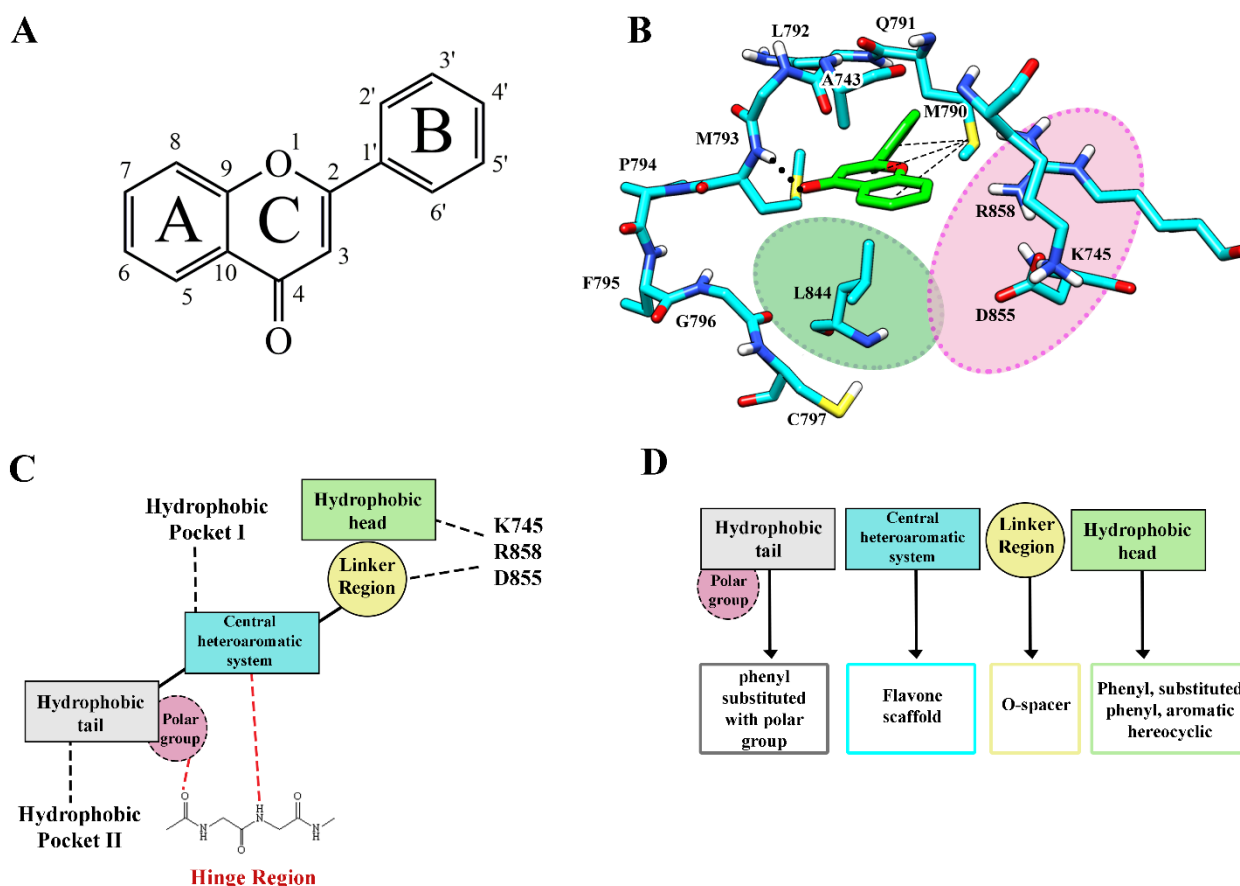
Figure 3. **(A)** Structure of the flavone. **(B)** Flavone-EGFR$^{L858R/T790M}$ complex in which the peripheral binding pocket and hydrophobic pocket II of the ATP-binding site is indicated with magenta and light green circles, respectively. **(C)** Rational for the drug design of new chemical scaffold for the development of mutant-selective TKIs and **(D)** summary of the possible chemical used in the virtual library generation.

3.2 Identification of the hit compounds by three-track virtual screening and kinase inhibition assay

Approximately 500 designed molecules are screened through the docking simulations in the ATP-binding pockets of the EGFR$^{L858R/T790M}$, EGFR$^{L858R/T790M//C797S}$ mutants, and the wild-type EGFR. This three-track virtual screening has been performed to identify potential mutant-selective inhibitors with binding free energies lower than -10 kcal/mol (strong binders) and higher than -7.0 kcal/mol (weak binders) with respect to mutants and wild type, respectively (**Figure 1**). The process has led to only two molecules that met our filtration criteria showing high binding affinities for the mutants with selectivity over the wild-type. This small number of virtual hits is due to the difficulty in discovering a new generation of reversible EGFR inhibitors that are selective only for the mutants. The identified hits compounds differ from each other only for the presence of a NO$_2$functional group (H-bond acceptor) in **4** and NH$_2$ in **5** (H-bond donor and acceptor) on the phenoxy moiety linked to the A

ring of the flavone core; they can therefore be prepared using the same synthetic route shown in **Scheme 1**. The key starting material 2,5-dihydroxyaceophenone **1** has been O-arylated with 4-fluoronitrobenzene in the presence of $Cs_2(CO)_3$ to obtain the 2-hydroxy-5-(4-nitrophenoxy)acetophenone **2**. The following crossed aldol condensation with the phenoxybenzaldehyde led to the (E)-1-(2-hydroxy-5-(4-nitrophenoxy)phenyl)-3-(3-phenoxyphenyl)prop-2-en-1-one **3** that in the presence of DMSO-I_2 was oxidized to obtain the nitro-derivate **4** with the target flavone skeleton. The use of Ni(acac)$_2$ and PMHS allows to selectively reduce the nitro group to obtain the 6-(4-aminophenoxy)-2-(3 phenoxyphenyl)-4H-chromen-4-one **5.**
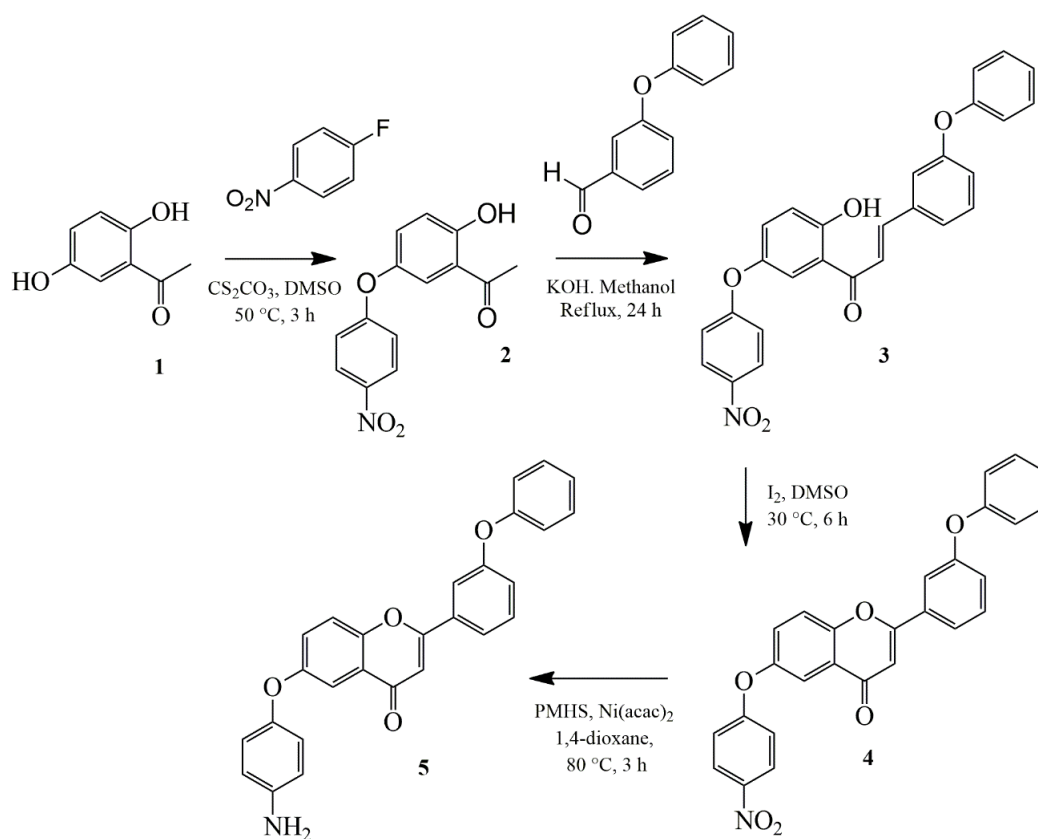
Scheme 1. Synthesis of selected compounds **4** and **5**.

Analysing the results obtained from the focused docking experiments, **4** shows a higher affinity for both mutants respect to **5** of about 1-2 kcal/mol (**Table 1**). Therefore, the corresponding calculated inhibitor constant value (K_i) of **5** is much higher than **4**.

Table 1. Population percentage, calculated binding affinity, K_i values obtained from focused docking and IC$_{50}$ values of inhibitors for selected compounds in complexes with mutants and wild type EGFR.
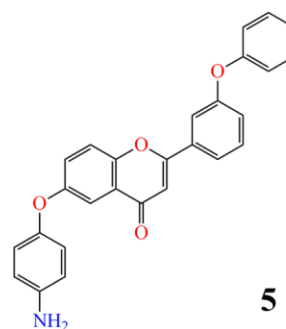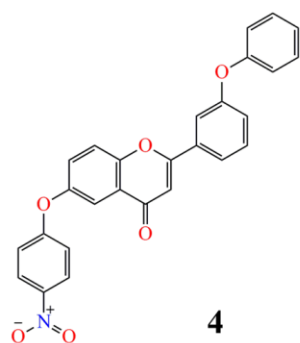
	Wild-type	L858R/T790M	L858R/T790M/C797S	Wild-type	L858R/T790M	L858R/T790M/C797S
Population (%)	81	72	83	99	45	99
Binding Affinity (kcal/mol)	- 5.9 ± 0.2	-10.6 ± 0.3	-11.2 ± 0.3	- 6.1 ± 0.3	-9.4 ± 0.1	-9.3 ± 0.2
Calculated K_i (nM)	374	24	17	305	128	166
Kinase activity (IC50, µM)	>150	12	16	>150	39	49

The *in silico* data agree with the *in vitro* inhibitory assay (**Table 1**). As shown, both compounds are selective for the mutants EGFR while sparing the wild-type one ($IC_{50} > 150$) underlying the efficacy of our drug design strategy. However, the best result is obtained with the nitro-derivative **4,** which inhibits the phosphorylation of EGFR mutant forms at low-micromolar concentration. This is particularly interesting because nitro-aromatics are incorporated within many approved drugs [40], including Chloramphenicol antibiotic [41], a hypnotic drug such as Flunitrazepam [42], and Venetoclax [43] which is used to treat chronic lymphocytic leukemia.

By examining the calculated binding mode of the selected hit **4** with the different EGFR mutate forms, it is possible to rationalize the observed mutant-selectivity (**Figure 5**) and how the $–NH_2$ group decreased the affinity for the EGFR[L858R/790M] and EGFR[L858R/790M/C797S] with respect to the presence of the $–NO_2$ moiety.
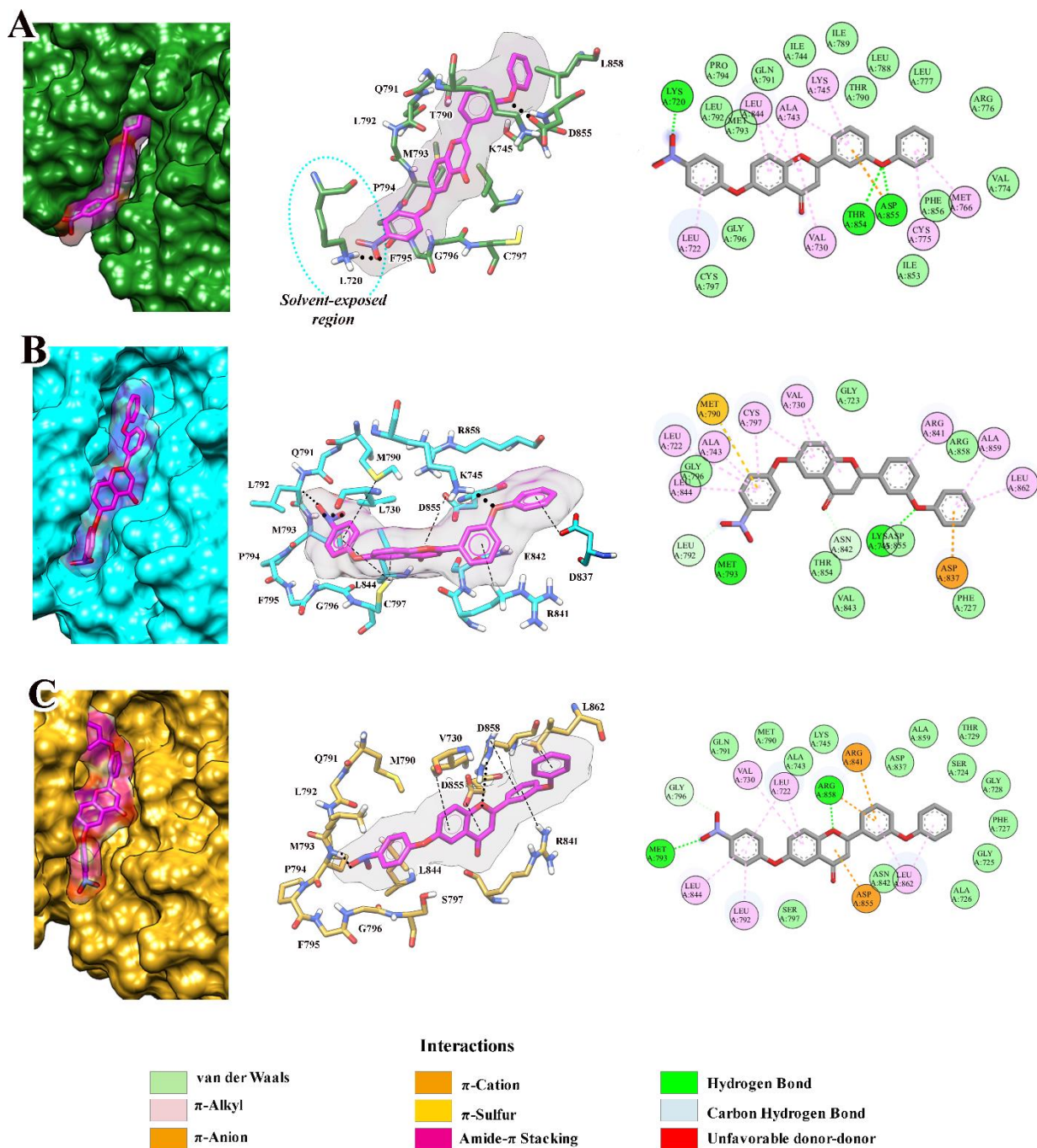
Figure 5. Focused docking of **4** in the ATP-binding site of **(A)** wild type EGFR (forest green), **(B)** EGFR[L858R/T790M] (cyan) and **(C)** EGFR[L858R/T790M/C797S] (golden rod). Carbon atoms of **4** are coloured in magenta. Hydrogen-bond and π-interactions are represented with black thick and thin dotted line lines, respectively. From left to right: surface representation of the ATP-binding pocket with inhibitor, detailed binding mode of **4** in complex with EGFR receptors and 2D diagram drawn by Discovery Studio 4.5 representing the main residue involved in **4**-binding.

In both EGFR mutants, **4** binds the ATP-binding pocket from the hinge to the PB region, showing a common interaction pattern in these EGFR forms (**Figure 5**). The nitro group in the *para* position of the phenoxy moiety anchors the inhibitor at the hinge region level as bidentate HB ligand forming a

N-H···O interaction with the backbone nitrogen atoms of M793 and a noncanonical C-H···O interaction with L792 (in EGFR[L858R/T790M]) and G796 (in EGFR[L858R/T790M/C797S]). Although the C-H···O hydrogen bonds are classified as weak interactions, several studies underlie their importance in the stabilization of the kinase inhibitor complexes [44,45] and their role in increasing the binding affinity of nitro compounds [46,47].

In addition, the terminal phenoxy moiety, linked to C'3 position of the B ring, is extended toward the peripheral binding pocket interacting with one or more targeted residues (K745, R858 and D855). As expected, the whole inhibitor binding mode is stabilized by non-covalent interactions involving the π-systems of the aromatic moieties. More in detail, regarding the **4**-EGFR[L858R/T790M] complex, the phenyl group in A is involved in a π-sulfur interaction with the mutated M790, and in a C-H/π bond with the hydrophobic clamp motif (A743, L844 and L722) and the C797 residue. All these forces contribute to direct the nitro group towards the hinge region level and allow it to make the previously mentioned bidentate HB. The phenyl B ring is instead stabilized by C-H/π interaction with residues L862 and A859 in the activation loop and by a π-anion bond with D837 of the highly conserved HRD motif. As planned, the O-spacer linker on the ring B acts as an H-acceptor atom establishing an N-H···O HB with the amino group of the K745 side chain; in addition, a VdW interaction with R858 and D855 is observed. Regarding the EGFR[L858R/T790M/C797S], the nitrophenoxy moiety is again stabilized by C-H/π interactions with the hydrophobic clamp motif (A743 and L722) and by L792, another residue of the hinge region. In this case, the calculated binding mode shows only a VdW interaction with mutated M790 while a direct involvement of R858 is observed. The amino group of the arginine side chain makes a HB with the O1 of the flavone core and a π-cation interaction with the phenyl B ring. In addition, D855 contributes to this association by establishing a π-anion interaction with $C_2=C_3$ π system of the flavone skeleton while any interaction is observed with K745. In the wild type EGFR, the nitrophenoxy moiety of **4** does not act as bidentate HB moiety with the hinge region moving instead toward the region exposed to the solvent. Therefore, we hypothesized that the interactions with mutated residues (M790, in EGFR[L858R/T790M], and R858, EGFR[L858R/T790M/C797S]), are the driving force of the mutants-selectivity inhibition. In both EGFR mutants, the replacement of the nitro- with amino-group prevents the anchoring of **5** at the hinge region level; therefore, adifferent positioning of the compound is observed (**Figure 6**).
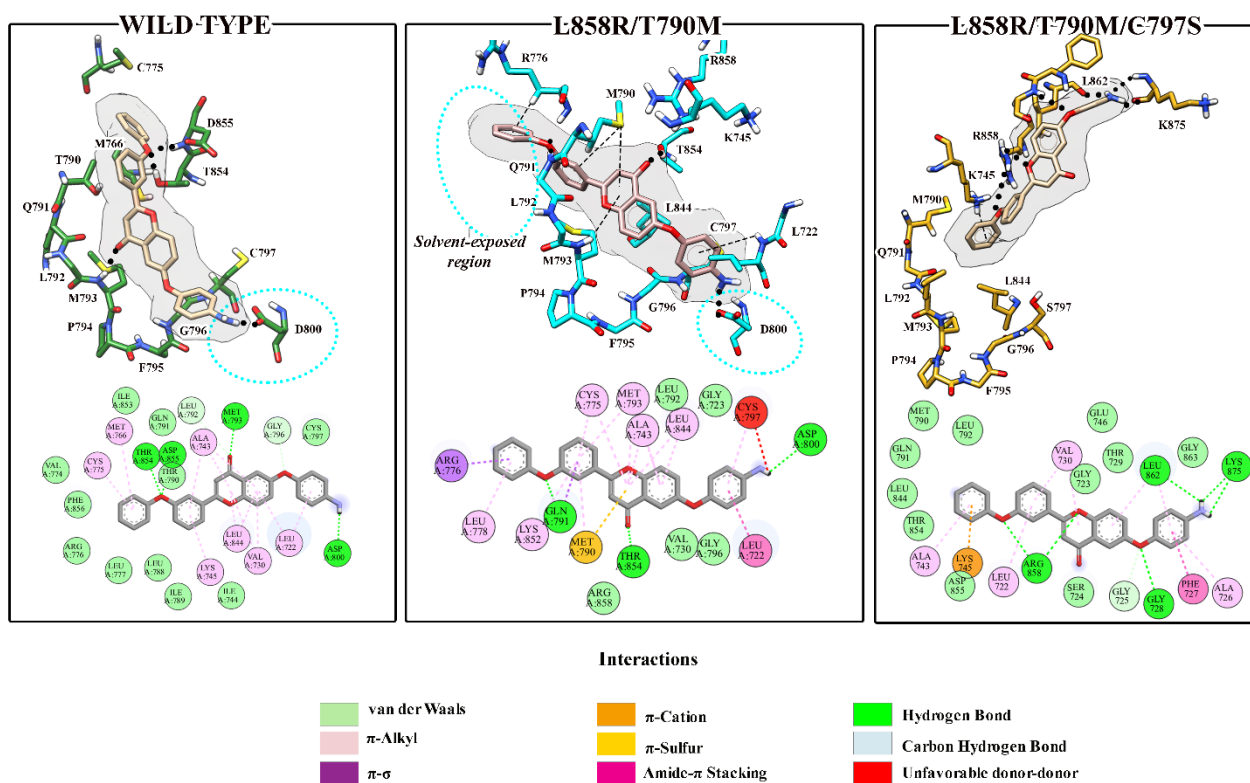
Figure 6. Detailed binding mode of **5** in complex with EGFR receptors and 2D diagram drawn by Discovery Studio 4.5 representing the main residue involved in **5**-binding. Carbon atoms of **5** are coloured in light brown. Hydrogen-bond and π-interactions are represented with black thick and thin dotted line lines, respectively. From left to right: surface representation of the ATP-binding pocket with inhibitor, detailed binding mode of **5** in complex with EGFR receptors and 2D diagram drawn by Discovery Studio 4.5 representing the main residue involved in **5**-binding.

However, the mutant-selectivity is again obtained by the specific interactions with the two mutated residues, M790 and R858. In fact, in the double mutant, the π-system of the flavone core makes key interactions involving M790 (π-sulfur and C-H/π), the hinge region residues M793 (C-H/π) and Q791 (π-σ). The terminal aminophenoxy moiety points instead toward a solvent-accessible region making a N-H···O HB with D800, which seems to be destabilized by the unfavourable donor-donor interaction with C797. It is worth noting that, any interaction with the phosphate binding pocket is observed in this case. Interestingly, in the triple mutant, the side chain of R858 shows a similar behaviour we observed for the **4** making an HB with the O1 of flavone core in addition to HB with the O-spacer at phenyl B ring level. However, **5** is localized mainly at the PB region, completely loosing the interaction with the hinge region. Overall, the absence of interactions with the PB region, in the EGFR$^{L858R/T790M}$, and with the hinge region, in the EGFR$^{L858R/T790M/C797S}$ can explain the decrease in IC$_{50}$ values for the nitro analogue **4** (**Table 1**).

3.3. Evaluation of binding mode stability by molecular dynamic simulations

To address the dynamic stability of the binding modes observed with docking experiments, we performed molecular dynamics (MD) simulations for EGFR$^{L858R/T790M}$ and EGFR$^{L858R/T790M/C797S}$ **4**-complexes. Using the trajectory snapshots, the root mean square deviations have been calculated from the initial structure (RMSD$_{init}$) of the backbone of the double and triple mutants (**Figure 7A**), and those for the heavy atoms of **4** (**Figure 7B**) to estimate the time evolutions of the protein conformation and the binding mode of **4**, respectively.
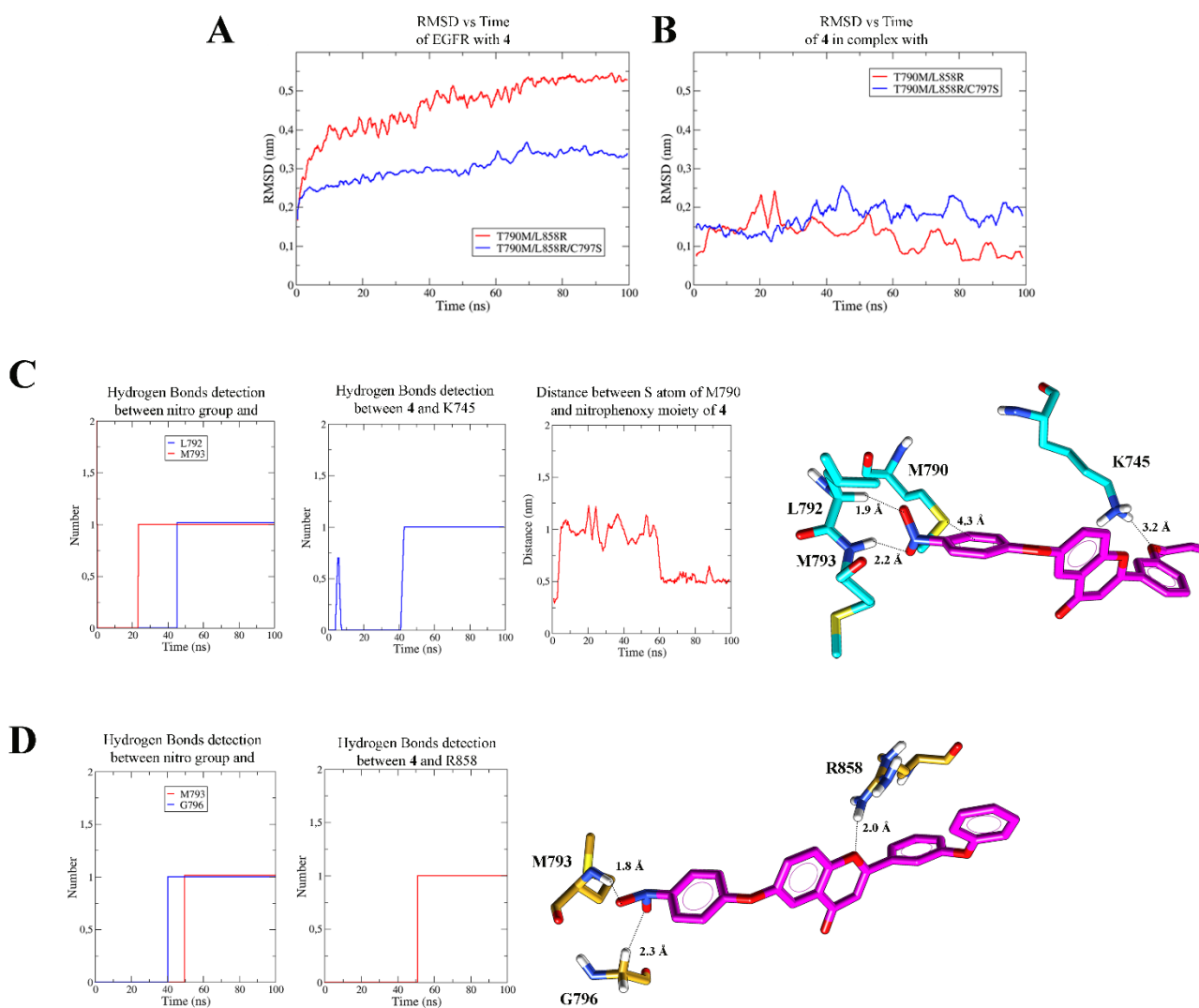

Figure 7. Root mean square deviation (RMSD) of (**A**) EGFR$^{L858R/T790M}$ and EGFR$^{L858R/T790M/C797S}$ and (**B**) of molecule **4** in complex with mutated receptors. (**C**) Time evolutions of the hydrogen-bond and π-sulfur interaction in the L858R/T790M-**4** complex involving the residues in the hinge region, K745 amino acid and M790. (**D**) Time evolutions of the hydrogen-bond in the L858R/T790M/C797S-**4** complex involving the residues in the hinge region and the side chain of R858 amino acid.

RMSD values detected for the EGFR forms highlight that different stabilization patterns can be observed for the complexes when C797S mutation occurs (**Figure 7A**). In fact, an evident decrease

in the RMSD values can be seen for the system with EGFR[L858R/T790M/C797S]. Nonetheless, it is worth mentioning that each system reached convergence after 60 ns of MD simulations, meaning that each complex finds a proper steady state, being both stabilised when molecule **4** binds the pocket. Monitoring the molecule behaviour (**Figure 7B**), even if little differences in the stabilization pathways are observed between the two models, the RMSD values always remain low undergoing only small fluctuations, remarking high stability in the binding pocket when this molecule binds both the EGFR mutated forms.

To verify that the HBs shown in **Figure 7C-D** would be the most significant binding forces for **4** to tightly bind in the ATP-binding site of the mutants, we monitored their presence along 100 ns of MD. After an initial stabilization, we observe in both EGFR mutants a constant presence of the bidentate HB with the hinge region. Both N-H···O interaction with the backbone nitrogen atoms of M793 and noncanonical C-H···O with L792 (in EGFR[L858R/T790M]) and G796 (in EGFR[L858R/T790M/C797S]) appear to be dynamically stable. In EGFR[L858R/T790M], we also evaluate the stability of π-sulphur interaction as the time evolutions of the distance from the sulphur atom of the mutated M790 to the centre of mass (CM) of the nitrophenoxy moiety linked to C6 of the A ring. Interestingly, this distance falls within 0.5 nm, which is considered the optimal inter-segment separation for π-sulfur interaction [48]. This dynamically stable hydrophobic contact with M790 could have the effect of positioning **4** to form the HBs in the hinge region of the L858R/T790M mutant (**Figure 5**). Regarding the EGFR[L858R/T790M/C797S] we monitor the maintenance of the HB involving the side chain of R858 and O1 of flavone core. The results show that after 50 ns of MD simulation this interaction is retained, leading us to assume that it represents the main force that guides the EGFR[L858R/T790M/C797S] inhibition.

3.4 Influence of phenoxy moieties on the inhibitory activity of nitroflavone 4

To find relationships between chemical structure and inhibitor activity of **4,** using a similar synthetic route to that described for **4** (Scheme 1), we synthetised flavone analogues that lack one of the two phenoxy moieties and in which the nitrophenoxy moiety placed in a different position in the A ring. Their kinase inhibitor activity has then been evaluated against the EGFR mutant forms; as control, we also evaluated the kinase inhibition actitivy of Lapatinib the well-known reversible TKI [49]. As shown in **Table 2**, the position shift (**4b, 4c**) of the nitrophenoxy moiety in the A ring of the flavone lead to the loss or decrease in the inhibitory activity. Interestingly, although with a lower potency, other mutant-active compound could be represented by **4a** in which we remove the phenoxy moiety linked to the C3' of the B ring. Overall, these findings are consistent with the critical role played by the C6-nitrophenoxy, which promote the formation of the strategic bidentate HB with the hinge

region, and that the C3'- phenoxy moiety is important to obtain a more efficient and potent EGFR inhibition.

Table 2. Structures of **4** analogues and their IC$_{50}$ values for the wild-type, L858R/T790M and L858R/T790M/C797S EGFR.
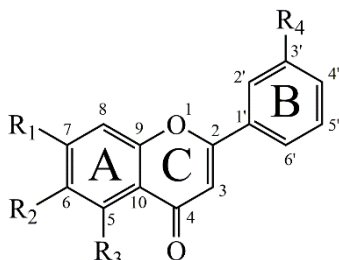
	Chemical substituent				Kinase activity (IC50, µM)		
Entry	R1	R2	R3	R4	Wild-type	L858R/T790M	L858R/T790M/C797S
LAPATINIB			-		0.005	12	> 20
4	H	O—(phenyl)—O$_2$N	H	O—phenyl	> 150	12	16
5	H	O—(phenyl)—NH$_2$	H	O—phenyl	> 150	39	49
4a	H	O—(phenyl)—O$_2$N	H	H	N.D.[a]	43	41
4b	O—(phenyl)—O$_2$N	H	H	O—phenyl	67	> 150	>150
4c	H	H	O—(phenyl)—O$_2$N	O—phenyl	106	> 150	73

[a] no significant inhibition was detected at the highest inhibitor concentration

Conclusion

Overall, the flavone-based compound **4** containing a nitrophenoxy group may act as an effective scaffold for designing novel generation EGFR inhibitors due to its low-micromolar inhibitory activity against EGFR$^{L858M/T790M}$ and EGFR$^{L858M/T790M/C797S}$ added to a good selectivity over the wild-type. Structural modifications focused on the terminal phenoxy moiety on the B ring could be explored to reinforce the interaction with the phosphate binding region. Starting from **4**, novel TKIs will be therefore designed to obtain molecules with nanomolar inhibitory activity and shed light on new strategies to overcome current T790M and C797S mediated resistance.

References

[1]   D.R. Camidge, W. Pao, L. v. Sequist, Acquired resistance to TKIs in solid tumours: Learning from lung cancer, Nat Rev Clin Oncol. 11 (2014) 473–481. https://doi.org/10.1038/nrclinonc.2014.104.

[2]   L.Y. Chen, M.A. Molina-Vila, S.Y. Ruan, K.Y. Su, W.Y. Liao, K.L. Yu, C.C. Ho, J.Y. Shih, C.J. Yu, J.C.H. Yang, R. Rosell, P.C. Yang, Coexistence of EGFR T790M mutation and common activating mutations in pretreatment non-small cell lung cancer: A systematic review and meta-analysis, Lung Cancer. 94 (2016) 46–53. https://doi.org/10.1016/j.lungcan.2016.01.019.

[3]   Y. Jia, C.H. Yun, E. Park, D. Ercan, M. Manuia, J. Juarez, C. Xu, K. Rhee, T. Chen, H. Zhang, S. Palakurthi, J. Jang, G. Lelais, M. DiDonato, B. Bursulaya, P.Y. Michellys, R. Epple, T.H. Marsilje, M. McNeill, W. Lu, J. Harris, S. Bender, K.K. Wong, P.A. Jänne, M.J. Eck, Overcoming EGFR(T790M) and EGFR(C797S) resistance with mutant-selective allosteric inhibitors, Nature. 534 (2016) 129–132. https://doi.org/10.1038/nature17960.

[4]   C. To, J. Jang, T. Chen, E. Park, M. Mushajiang, D.J.H. de Clercq, M. Xu, S. Wang, M.D. Cameron, D.E. Heppner, B.H. Shin, T.W. Gero, A. Yang, S.E. Dahlberg, K.K. Wong, M.J. Eck, N.S. Gray, P.A. Jänne, Single and dual targeting of mutant egfr with an allosteric inhibitor, Cancer Discov. 9 (2019) 926–943. https://doi.org/10.1158/2159-8290.CD-18-0903.

[5]   X. Du, B. Yang, Q. An, Y.G. Assaraf, X. Cao, J. Xia, Acquired resistance to third-generation EGFR-TKIs and emerging next-generation EGFR inhibitors, The Innovation. 2 (2021). https://doi.org/10.1016/j.xinn.2021.100103.

[6]   S.N. Milik, D.S. Lasheen, R.A.T. Serya, K.A.M. Abouzid, How to train your inhibitor: Design strategies to overcome resistance to Epidermal Growth Factor Receptor inhibitors, Eur J Med Chem. 142 (2017) 131–151. https://doi.org/10.1016/j.ejmech.2017.07.023.

[7]   F. Ferlenghi, L. Scalvini, F. Vacondio, R. Castelli, N. Bozza, G. Marseglia, S. Rivara, A. Lodola, S. la Monica, R. Minari, P.G. Petronini, R. Alfieri, M. Tiseo, M. Mor, A sulfonyl fluoride derivative inhibits EGFRL858R/T790M/C797S by covalent modification of the catalytic lysine, Eur J Med Chem. 225 (2021). https://doi.org/10.1016/j.ejmech.2021.113786.

[8]   D.E. Heppner, M. Günther, F. Wittlinger, S.A. Laufer, M.J. Eck, Structural Basis for EGFR Mutant Inhibition by Trisubstituted Imidazole Inhibitors, J Med Chem. 63 (2020) 4293–4305. https://doi.org/10.1021/acs.jmedchem.0c00200.

[9]   T. Amelia, R.E. Kartasasmita, T. Ohwada, D.H. Tjahjono, Structural Insight and Development of EGFR Tyrosine Kinase Inhibitors, Molecules. 27 (2022). https://doi.org/10.3390/molecules27030819.

[10]   C.-H. Yun, T.J. Boggon, Y. Li, M.S. Woo, H. Greulich, M. Meyerson, M.J. Eck, M. Eck, Structures of lung cancer-derived EGFR mutants and inhibitor complexes: Mechanism of activation and insights into differential inhibitor sensitivity, Cancer Cell. 11 (2007) 217–227.

[11]   M. Günther, J. Lategahn, M. Juchum, E. Doering, M. Keul, J. Engel, H.L. Tumbrink, D. Rauh, S.A. Laufer, Trisubstituted Pyridinylimidazoles as Potent Inhibitors of the Clinically Resistant L858R/T790M/C797S EGFR Mutant: Targeting of Both Hydrophobic Regions and the Phosphate Binding Site, J. Med. Chem., Just Accepted Manuscript • Publication Date. (2017). http://pubs.acs.org.

[12]   Y.H. Peng, H.Y. Shiao, C.H. Tu, P.M. Liu, J.T.A. Hsu, P.K. Amancha, J.S. Wu, M.S. Coumar, C.H. Chen, S.Y. Wang, W.H. Lin, H.Y. Sun, Y.S. Chao, P.C. Lyu, H.P. Hsieh, S.Y. Wu, Protein kinase inhibitor design by targeting the Asp-Phe-Gly (DFG) motif: The role of the DFG motif in the design of epidermal growth factor receptor inhibitors, J Med Chem. 56 (2013) 3889–3903. https://doi.org/10.1021/jm400072p.

[13]   S. Sogabe, Y. Kawakita, S. Igaki, H. Iwata, H. Miki, D.R. Cary, T. Takagi, S. Takagi, Y. Ohta, T. Ishikawa, Structure-based approach for the discovery of pyrrolo[3,2- d]pyrimidine-based EGFR T790M/L858R mutant inhibitors, ACS Med Chem Lett. 4 (2013) 201–205. https://doi.org/10.1021/ml300327z.

[14]   J. Ko, H. Park, L. Heo, C. Seok, GalaxyWEB server for protein structure prediction and refinement, Nucleic Acids Res. 40 (2012). https://doi.org/10.1093/nar/gks493.

[15]   A. Ceroni, A. Passerini, A. Vullo, P. Frasconi, Disulfind: A disulfide bonding state and cysteine connectivity prediction server, Nucleic Acids Res. 34 (2006). https://doi.org/10.1093/nar/gkl266.

[16]   E.F. Pettersen, T.D. Goddard, C.C. Huang, G.S. Couch, D.M. Greenblatt, E.C. Meng, T.E. Ferrin, UCSF Chimera - A visualization system for exploratory research and analysis, J Comput Chem. 25 (2004) 1605–1612. https://doi.org/10.1002/jcc.20084.

[17]   A. v. Onufriev, G. Sigalov, A strategy for reducing gross errors in the generalized Born models of implicit solvation, Journal of Chemical Physics. 134 (2011). https://doi.org/10.1063/1.3578686.

[18]   G.M. Morris, H. Ruth, W. Lindstrom, M.F. Sanner, R.K. Belew, D.S. Goodsell, A.J. Olson, Software news and updates AutoDock4 and AutoDockTools4: Automated docking with selective receptor flexibility, J Comput Chem. 30 (2009) 2785–2791. https://doi.org/10.1002/jcc.21256.

[19]   M.F. Sanner, B.S. Duncan, C.J. Carrillo, A.J. Olson, INTEGRATING COMPUTATION AND VISUALIZATION FOR BIOMOLECULAR ANALYSIS: AN EXAMPLE USING PYTHON AND AVS, Pacific Symposium on Biocomputing. 4 (1999) 392–400.

[20]   Z. Zhao, L. Xie, P.E. Bourne, Structural Insights into Characterizing Binding Sites in Epidermal Growth Factor Receptor Kinase Mutants, J Chem Inf Model. 59 (2019) 453–462. https://doi.org/10.1021/acs.jcim.8b00458.

[21]   C. Minnelli, E. Laudadio, G. Mobbili, R. Galeazzi, Conformational insight on WT-and mutated-EGFR receptor activation and inhibition by epigallocatechin-3-gallate: Over a rational basis for the design

of selective non-small-cell lung anticancer agents, Int J Mol Sci. 21 (2020). https://doi.org/10.3390/ijms21051721.

[22]   E. Laudadio, G. Mobbili, L. Sorci, R. Galeazzi, C. Minnelli, Mechanistic insight toward EGFR activation induced by ATP: role of mutations and water in ATP binding patterns, J Biomol Struct Dyn. (2022). https://doi.org/doi.org/10.1080/07391102.2022.2108497.

[23]   K. Stierand, P.C. Maaß, M. Rarey, Molecular complexes at a glance: Automated generation of two-dimensional complex diagrams, Bioinformatics. 22 (2006) 1710–1716. https://doi.org/10.1093/bioinformatics/btl150.

[24]   J. Huang, S. Rauscher, G. Nawrocki, T. Ran, M. Feig, B.L. de Groot, H. Grubmüller, A.D. MacKerell, CHARMM36m: An improved force field for folded and intrinsically disordered proteins, Nat Methods. 14 (2016) 71–73. https://doi.org/10.1038/nmeth.4067.

[25]   D. van der Spoel, E. Lindahl, B. Hess, G. Groenhof, A.E. Mark, H.J.C. Berendsen, GROMACS: Fast, flexible, and free, J Comput Chem. 26 (2005) 1701–1718. https://doi.org/10.1002/jcc.20291.

[26]   M.J. Abraham, T. Murtola, R. Schulz, S. Páll, J.C. Smith, B. Hess, E. Lindah, Gromacs: High performance molecular simulations through multi-level parallelism from laptops to supercomputers, SoftwareX. 1–2 (2015) 19–25. https://doi.org/10.1016/j.softx.2015.06.001.

[27]   S. Páll, B. Hess, A flexible algorithm for calculating pair interactions on SIMD architectures, Comput Phys Commun. 184 (2013) 2641–2650. https://doi.org/10.1016/j.cpc.2013.06.003.

[28]   T. Darden, D. York, L. Pedersen, Particle mesh Ewald: An N-log(N) method for Ewald sums in large systems, J. Chem. Phys. 98 (1993) 10089–10092.

[29]   S. Nose, A unified formulation of the constant temperature molecular dynamics methods, J. Chem. Phys. 81 (1984) 511–519. http://jcp.aip.org/about/rights_and_permissions.

[30]   M. Parrinello, A. Rahman, Polymorphic transitions in single crystals: A new molecular dynamics method, J. Appl. Phys. 25 (1981) 7182–7190. http://jap.aip.org/about/rights_and_permissions.

[31]   W. Humphrey, A. Dalke, K. Schulten, VMD: Visual Molecular Dynamics, J Mol Graph. 14 (1996) 33–38.

[32]   P. Zucchiatti, G. Birarda, A. Cerea, M.S. Semrau, A. Hubarevich, P. Storici, F. de Angelis, A. Toma, L. Vaccari, Binding of tyrosine kinase inhibitor to epidermal growth factor receptor: Surface-enhanced infrared absorption microscopy reveals subtle protein secondary structure variations, Nanoscale. 13 (2021) 7667–7677. https://doi.org/10.1039/d0nr09200b.

[33]   P.M. Murray, F. Bellany, L. Benhamou, D.K. Bučar, A.B. Tabor, T.D. Sheppard, The application of design of experiments (DoE) reaction optimisation and solvent selection in the development of new synthetic chemistry, Org Biomol Chem. 14 (2016) 2373–2384. https://doi.org/10.1039/c5ob01892g.

[34]   X. Wang, B. Chen, D. Xu, Z. Li, H. Liu, Z. Huang, K. Huang, X. Lin, H. Yao, Molecular mechanism and pharmacokinetics of flavonoids in the treatment of resistant EGF receptor-mutated non-small-cell lung cancer: A narrative review, Br J Pharmacol. 178 (2021) 1388–1406. https://doi.org/10.1111/bph.15360.

[35]   M. Cushman, H. Zhu, R.L. Geahlen, A.J. Kraker, Synthesis and Biochemical Evaluation of a Series of Aminoflavones as Potential Inhibitors of Protein-Tyrosine Kinases p56lck, EGFr, and p60v-src, J. Med. Chem. 37 (1994) 3353–3362. https://pubs.acs.org/sharingguidelines.

[36]   I. Ahmad, M. Shaikh, S. Surana, A. Ghosh, H. Patel, p38α MAP kinase inhibitors to overcome EGFR tertiary C797S point mutation associated with osimertinib in non-small cell lung cancer (NSCLC): emergence of fourth-generation EGFR inhibitor, J Biomol Struct Dyn. 40 (2022) 3046–3059. https://doi.org/10.1080/07391102.2020.1844801.

[37]   A.A. Gaber, A.H. Bayoumi, A.M. El-morsy, F.F. Sherbiny, A.B.M. Mehany, I.H. Eissa, Design, synthesis and anticancer evaluation of 1H-pyrazolo[3,4-d]pyrimidine derivatives as potent EGFR WT and EGFR T790M inhibitors and apoptosis inducers, Bioorg Chem. 80 (2018) 375–395. https://doi.org/10.1016/j.bioorg.2018.06.017.

[38]   H. Park, H.-Y. Jung, S. Mah, S. Hong, Discovery of EGF Receptor Inhibitors That Are Selective for the d746 - 750/T790M/C797S Mutant through Structure-Based de Novo Design , Angewandte Chemie. 56 (2017) 7634–7638. https://doi.org/10.1002/ange.201703389.

[39]   R.K. Raju, J.W.G. Bloom, Y. An, S.E. Wheeler, Substituent effects on non-covalent interactions with aromatic rings: Insights from computational chemistry, ChemPhysChem. 12 (2011) 3116–3130. https://doi.org/10.1002/cphc.201100542.

[40]   S. Noriega, J. Cardoso-Ortiz, A. López-Luna, M.D.R. Cuevas-Flores, J.A. Flores De La Torre, The Diverse Biological Activity of Recently Synthesized Nitro Compounds, Pharmaceuticals. 15 (2022) 717. https://doi.org/10.3390/ph15060717.

[41]   P. Arno, R. Ashley, P. Bames, D. Brown, D. Burke, K. Brudney, R. Bumgarner, G. Cauthen, J. Cook, A. Dannenberg, S. Dooley, M. Earle, D. Enarson, P. Fine, T. Frieden, L. Garrett, D. Gwynn, M. Hamburg, G. Hardy, C. Hayden, J. Hill, P. Hopewell, M. Iseman, W. Jacobs, A. Kochi, L. Reichman, A. Rouillon, C. Schieffelbein, G. School-Nik, J. Schwartz, P. Smith, D. Snider, S. Spinacci, K. Styblo, H.C. Neu, The Crisis in Antibiotic Resistance, Science (1979). 257 (1992) 1064–1072. www.sciencemag.org.

[42]   J.A. Davies Bath, Flunitrazepam, 2009.

[43]   A.W. Roberts, M.S. Davids, J.M. Pagel, B.S. Kahl, S.D. Puvvada, J.F. Gerecitano, T.J. Kipps, M.A. Anderson, J.R. Brown, L. Gressick, S. Wong, M. Dunbar, M. Zhu, M.B. Desai, E. Cerri, S. Heitner Enschede, R.A. Humerickhouse, W.G. Wierda, J.F. Seymour, Targeting BCL2 with Venetoclax in Relapsed Chronic Lymphocytic Leukemia, New England Journal of Medicine. 374 (2016) 311–322. https://doi.org/10.1056/nejmoa1513257.

[44]   A.C. Pierce, K.L. Sandretto, G.W. Bemis, Kinase inhibitors and the case for CH···O hydrogen bonds in protein-ligand binding, Proteins: Structure, Function and Genetics. 49 (2002) 567–576. https://doi.org/10.1002/prot.10259.

[45]   S.K. Panigrahi, Strong and weak hydrogen bonds in protein-ligand complexes of kinases: A comparative study, Amino Acids. 34 (2008) 617–633. https://doi.org/10.1007/s00726-007-0015-4.

[46]   H. Steuber, A. Heine, G. Klebe, Structural and Thermodynamic Study on Aldose Reductase: Nitro-substituted Inhibitors with Strong Enthalpic Binding Contribution, J Mol Biol. 368 (2007) 618–638. https://doi.org/10.1016/j.jmb.2006.12.004.

[47]   A. Jezuita, K. Ejsmont, H. Szatylowicz, Substituent effects of nitro group in cyclic compounds, Struct Chem. 32 (2021) 179–203. https://doi.org/10.1007/s11224-020-01612-x/Published.

[48]   A.L. Ringer, A. Senenko, C.D. Sherrill, Models of S/π interactions in protein structures: Comparison of the H 2 S-benzene complex with PDB data , Protein Science. 16 (2007) 2216–2223. https://doi.org/10.1110/ps.073002307.

[49] D. Li, L. Ambrogio, T. Shimamura, S. Kubo, M. Takahashi, L.R. Chirieac, R.F. Padera, G.I. Shapiro, A. Baum, F. Himmelsbach, W.J. Rettig, M. Meyerson, F. Solca, H. Greulich, K.K. Wong, BIBW2992, an irreversible EGFR/HER2 inhibitor highly effective in preclinical lung cancer models, Oncogene. 27 (2008) 4702–4711. https://doi.org/10.1038/onc.2008.109.